Pure Appl. Chem., Vol. 79, No. 10, pp. 1643–1652, 2007.
doi:10.1351/pac200779101643

Structure and dynamics of levitated liquid materials*

Louis Hennet[1,‡], Shankar Krishnan[2], Irina Pozdnyakova[1], Viviana Cristiglio[3], Gabriel J. Cuello[3], Henry E. Fischer[3], Aleksei Bytchkov[4], Francesco Albergamo[4], Didier Zanghi[1], Jean-François Brun[1], Séverine Brassamin[1], Marie-Louise Saboungi[5], and David L. Price[1]

[1]CNRS-CRMHT, 1d avenue de la Recherche Scientifique, 45071 Orléans, Cedex 2, France; [2]Tencor, San Jose, CA USA; [3]ILL, BP 156, 38042 Grenoble, Cedex 9, France; [4]ESRF, BP 220, 38043 Grenoble, Cedex, France; [5]CRMD, 1b rue de la Férollerie, 45071 Orléans, Cedex 2, France

Abstract: Aerodynamic levitation is a simple way to suspend samples which can be heated with CO_2 lasers. The advantages of this technique are the simplicity and compactness of the device, making it possible to integrate the device easily into different kinds of experiments. In addition, all types of sample can be used, including metals and oxides. The integration of this technique at synchrotron and neutron sources provides powerful tools to study molten materials.

Keywords: aerodynamic levitation; synchrotron spectroscopy; neutron scattering; containerless techniques; molten metal; molten oxide.

INTRODUCTION

Studies of the liquid state present an obvious fundamental interest and are also important for technological applications since the molten state is an essential stage in various industrial processes (glass making, single-crystal growing, iron- and steel-making industry…).

Most of the physical properties of a high-temperature liquid are related to its atomic structure. Thus, it is important to develop devices to probe the local environment of the atoms in the sample. At very high temperature, it is difficult to use conventional furnaces, which present several problems. In particular, the sample can be polluted by the container and the structural properties of the materials can be affected by the crucible. This has led to the development of containerless techniques and their use at synchrotron and neutron sources to study the structure and dynamics of molten materials.

CONTAINERLESS TECHNIQUES

Levitation methods

Levitation techniques are useful tools to study the structure and dynamics of high-temperature melts. In particular, they eliminate the problems of container interactions and contamination, making it possible

*Paper based on a presentation at the 12th International IUPAC Conference on High Temperature Materials Chemistry (HTMC-XII), 18–22 September 2006, Vienna, Austria. Other presentations are published in this issue, pp. 1635–1778.

‡Corresponding author: E-mail: hennet@cnrs-orleans.fr

to study the sample with a very high degree of control and to access very high temperatures. An additional advantage of the containerless method is that it is possible to supercool hot liquids several hundreds of degrees below their equilibrium freezing point.

Different levitation techniques have been developed by various groups around the world, and we give a short description of the principal methods.

Electromagnetic levitation [1] is one of the oldest techniques used for containerless experiments. In this case, a radio-frequency electromagnetic field is generated by a levitation coil. Then, Foucault currents are induced in the sample. This leads to an inductive heating of the sample and at the same time, the interaction of the Foucault currents with the magnetic field of the coil leads to a force that counteracts the gravity and makes it possible to levitate the sample. The levitation coil is situated in a vacuum chamber which is first evacuated and then filled with a very high purity gas, usually He or a mixture He + H_2 (few percents). The temperature of the sample is controlled by varying a gas flow arriving onto the sample through a ceramic tube. With this technique, the sample must be an electrical conductor (metals or semiconductors).

With electrostatic levitation [2], the sample is electrically charged and levitated in a vertical electrostatic field between two electrodes. Two pairs of smaller side electrodes are used to position the sample horizontally. When it levitates, the sample can be heated using lasers. With this method, it is possible to study all samples that can be electrically charged. This method has various advantages. First, it works under vacuum, preventing contamination, and it makes it possible to study bad electrical conductors or materials with low melting point. One drawback is the complexity of the set-up that limits its combination with various spectroscopies. While some insulating oxides can be studied with this technique, it is mostly used with metals.

The acoustic levitation [3] uses an acoustic wave that is used to counteract the gravity, and as previously, the sample can be heated using lasers.

With the gas film levitation technique [4], the sample is levitated by floating on a thin gas film formed by a gas flow passing through a porous membrane. The typical thickness of the gas film is between 10 and 100 μm. With this technique, it is possible to levitate a large amount of material (a few grams), which can be heated using a furnace, for instance.

At CRMHT, we have chosen to work with the aerodynamic levitation method associated with CO_2 laser heating [5,6]. The advantages are the simplicity and compactness of the device, making it possible to integrate the device easily in different experimental set-ups. Some devices developed at neutron and synchrotron sources will be presented.

Temperature measurements

With levitation techniques, optical pyrometry is the ideal method for temperature measurements. This technique is very easy to use but requires emissivity corrections to derive the true temperature, T, from the apparent temperature T_a measured by the pyrometer:

$$\frac{1}{T} - \frac{1}{T_a} = \frac{\lambda}{C_2} \ln\left(\varepsilon_\lambda\right) \tag{1}$$

where C_2 = 1.4388 cm. K is the Planck's second radiation constant and ε_λ is the spectral emissivity of the material at the used pyrometer wavelength λ.

STRUCTURE OF LIQUID MATERIALS

X-ray and neutron scattering techniques are important sources of structural information on molten materials through the determination of the structure factor $S(Q)$ and the calculation of the corresponding pair correlation function $g(r)$. Over the past 10 years, the combination of containerless techniques with

X-ray diffraction at synchrotron sources has enabled structural investigations of various materials above the melting point and in the supercooled state [7,8]. More recently, neutron diffraction has been applied to the study of levitated liquids [9]. In the following paragraph, we detail these two techniques and show some recent results.

Theoretical background

A detailed description of the technique and theoretical background for X-ray and neutron diffraction from liquids and glasses can be found in Fischer et al. [10]. In an X-ray diffraction experiment from an *n*-component material, the mean differential scattering cross-section per atom can be written as:

$$\frac{d\sigma}{d\Omega} = \sum_{i=1}^{n} c_i \left|f_i\right|^2 + \left|\sum_{i=1}^{n} c_i f_i\right|^2 \left(S(Q) - 1\right) \tag{2}$$

where c_i and f_i are, respectively, the atomic concentration and the atomic scattering factors of species i present in the sample. $f_i = f_i^0 + f_i' + if_i''$ is a complex quantity containing anomalous dispersion coefficients f_i' and f_i''. All these values are tabulated [11,12]. With neutrons, the f_i are replaced by the coherent scattering length b_i. The b_i values have been compiled by Sears [13]. The pair correlation function $g(r)$ is calculated from $S(Q)$ using a classical Fourier transform:

$$g(r) = 1 + \frac{1}{2\pi^2 \rho_0} \int_0^{Q_{\max}} Q(S(Q) - 1) \frac{\sin Qr}{r} dQ \tag{3}$$

where ρ_0 is the number of atoms per unit volume. Like $S(Q)$, $g(r)$ is a weighted sum of partial functions:

$$g(r) = \sum_{i,j} \frac{c_i c_j f_i f_j^*}{\left|\sum c_i f_i\right|^2} g_{ij}(r) \tag{4}$$

Experimental set-up for X-ray scattering

X-ray diffraction experiments have been carried out at various synchrotron sources using different set-ups. We describe here the levitation set-up installed at the ID-11-C beamline at the Advance Photon Source (APS) in Argonne, IL, USA. This beamline is situated on a multipole wiggler providing an intense X-ray beam. Since it is largely described elsewhere [14], we give only a brief description of the apparatus (illustrated in Fig. 1).

The levitation chamber is mounted at the center of the goniometer. A spherical sample (3 mm in diameter) is levitated by a gas flow going through a nozzle situated in the center of the chamber. A mass flow controller enables an accurate regulation of the gas flow. For experiments on liquid metals, the chamber is evacuated, filled with high-purity argon and then purged for short durations with a gas flow. A pressure regulation system maintains the chamber at a pressure around 500 mbar. The argon gas flow is about 0.3 l/min.

The heating system is constituted by a 270-W CO_2 laser (λ = 10.6 μm) directed at the sample with two mirrors through a ZnSe window.

Two optical pyrometers are employed simultaneously. The first one operates at 0.65 μm, and the second in the 1–2.5 μm band pass. The pyrometers are oriented at 45° on either side of the vertical plane and are focused at a point on the surface of the specimen close to the illumination point of the X-ray beam.

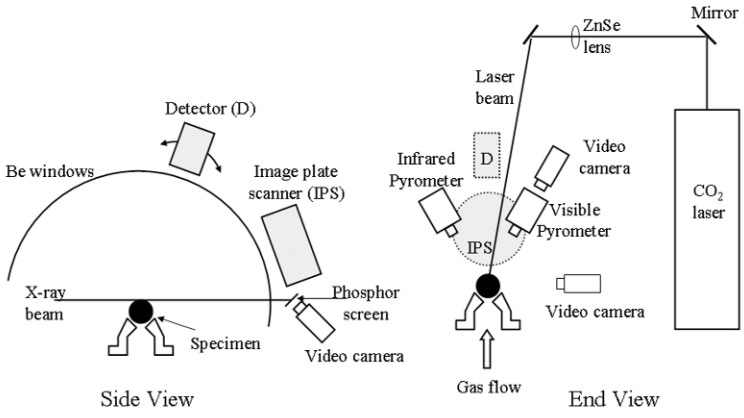

Fig. 1 Schematic view of the experimental arrangement at APS.

A precise sample positioning is achieved by means of a motorized translation stage nozzle and using a phosphor screen in front of a video camera to observe the shadow of the specimen in the X-ray beam.

The diffracted beam is detected using a germanium solid-state detector scanned over wide angular range.

Experimental set-up for neutron scattering

It is also interesting to have the possibility to combine X-ray and neutron scattering experiments. Figure 2 is a schematic view of the levitation set-up integrated into the D4c spectrometer [15] at the Institut Laue-Langevin (ILL) in Grenoble, France. This system is an evolution of our first device developed for the SANDALS station at ISIS [16] (Rutherford Laboratory, UK).

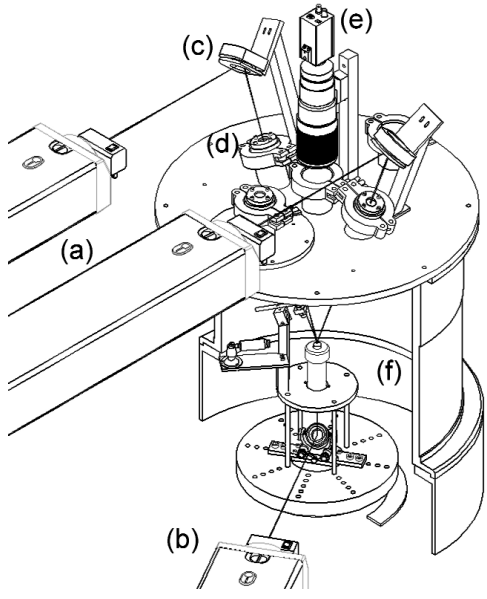

Fig. 2 Schematic view of the experimental arrangement: laser heads (a,b), spherical mirrors (c), NaCl windows, (d) video camera (e), and levitation device (f).

The samples are heated to the desired temperatures by two 125-W CO_2 lasers directed from above. The laser beams are focused on the sample by means of spherical mirrors at two different angles in order to obtain a homogeneous temperature distribution. Two NaCl windows are used to transmit the beam into the vacuum chamber. The pyrometer is placed inside the chamber to avoid window corrections. A third laser directed at the sample from below through the nozzle is used to compensate the cooling of the sample by the gas flow. A high-quality video image of the sample taken from above is continuously displayed in order to monitor the sample levitation during heating. Video images of the sample are also recorded with a horizontal camera in order to determine the sample position in the levitator and to monitor the vertical stability.

Structure of liquid metals

In this section, we present a structural study of liquid Zr using X-rays. In order to avoid fluorescence effects, scattering measurements were made at an X-ray energy of 17.9 keV, just below the Zr Kα absorption edge (17.998 keV). We used an angular range of 2–105°, giving a maximum value for the scattering vector $\boldsymbol{Q}$ of 14.4 $Å^{-1}$.

The X-ray structure factors for liquid Zr are plotted in Fig. 3a at four temperatures above the melting point (2128 K): 2200, 2325, 2446, and 2580 K. All curves are very similar, showing that there is no important structural evolution with the temperature. They are characterized by a main peak at 2.4 $Å^{-1}$ followed by a broader second peak centered at 4.45 $Å^{-1}$. There is also a weaker third peak around 6.5 $Å^{-1}$.

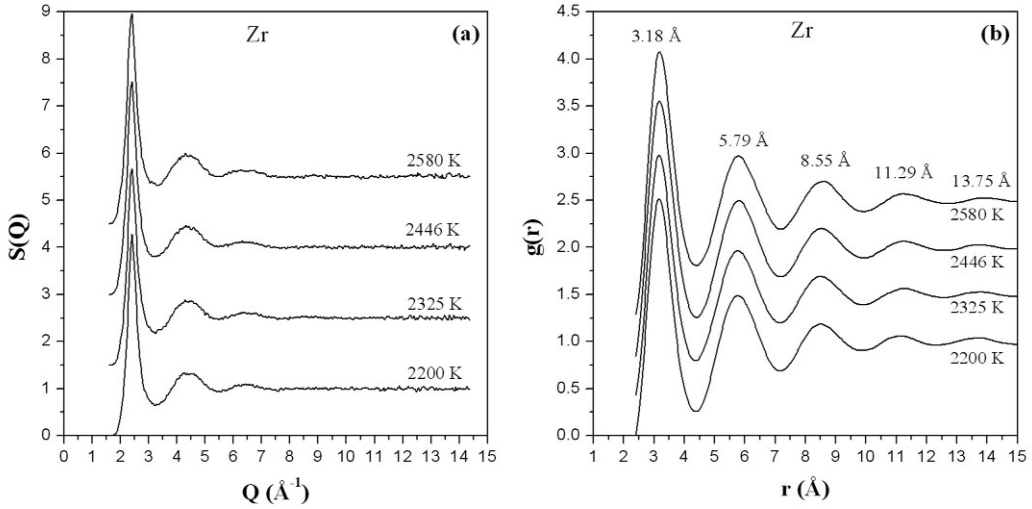

Fig. 3 (a) X-ray structure factor $S(Q)$ for liquid Zr at various temperature above the melting point. (b) Corresponding X-ray pair correlation functions $g(r)$ at the same temperature. In both cases, curves are shifted up for clarity.

Figure 3b shows the pair correlation function at the same four temperatures obtained by a Fourier transform of $S(Q)$ using eq. 3. All curves exhibit five well-defined peaks centered at 3.18, 5.79, 8.55, 11.89, and 13.75 Å. Integration under the first peak in all $g(r)$ gives similar coordination numbers from 12.5 ± 0.5 at 2580 K to 12.3 ± 0.5 at 2200 K. This very slight variation with decreasing temperature does not allow any conclusion. In addition, an inverted behavior has been found with a neutron-scattering experiment [17]. In the solid, Zr has a hexagonal closed-packed (hcp) structure (P63/mmc space group) with lattice parameters $a = b = 3.23$ Å and $c = 5.14$ Å. It is then possible to calculate the first in-

teratomic distances. For the five first we find 3.17, 3.23, 4.53, 5.14, and 5.56 Å. These interatomic distances are very close to those obtained in the liquid state. This shows that the liquid structure is very similar to the solid one.

Structure of liquid refractory oxides

With a pure element as previously, it is relatively easy to determine distances and coordination numbers. In this section, we will see that the data interpretation becomes more complicated with multicomponent materials. We present in the following a combined X-ray and neutron study or liquid YAG ($Y_3Al_5O_{12}$) above its melting point (2220 K).

The interest in studying the liquid properties of YAG arises from the fact that when it is doped with rare earths, it can be used in pumped lasers [18] or in scintillators [19]. YAG crystals are grown from the melt that requires a precise control of the growth conditions. It is then important to study the thermophysical properties that are related to the structure of the material at the atomic scale.

X-ray measurements were made at an energy of 16.75 keV, below the Y Kα absorption edge (17.038 keV). We used an angular range of 2–105°, giving a maximum value for the scattering vector $\boldsymbol{Q}$ of 13.5 $Å^{-1}$. The neutron data were obtained at a wavelength of 0.5 Å (~24.8 keV) in a 5–135° angular range, which gave a usable Q-range of 0.2–23.2 $Å^{-1}$.

Figure 4a shows the X-ray and neutron structure factors $S^X(Q)$ and $S^N(Q)$ of liquid YAG at a temperature of 2373 K. Both curves exhibit several peaks. In $S^N(Q)$, the first peak around 2.1 $Å^{-1}$ is very small compared to the corresponding peak at 2.13 $Å^{-1}$ in $S^X(Q)$. If we have a look at the weighting factors for neutron and X-rays (Table 1), it means that this peak is mostly due to Y-Y, Y-Al, and Al-Al correlations that have relatively low neutron weighting factors compared to X-rays, respectively, 13.5 and 41.1 %. The second peak at 2.86 $Å^{-1}$ in the neutron $S(Q)$ is mostly due to O-O correlations.

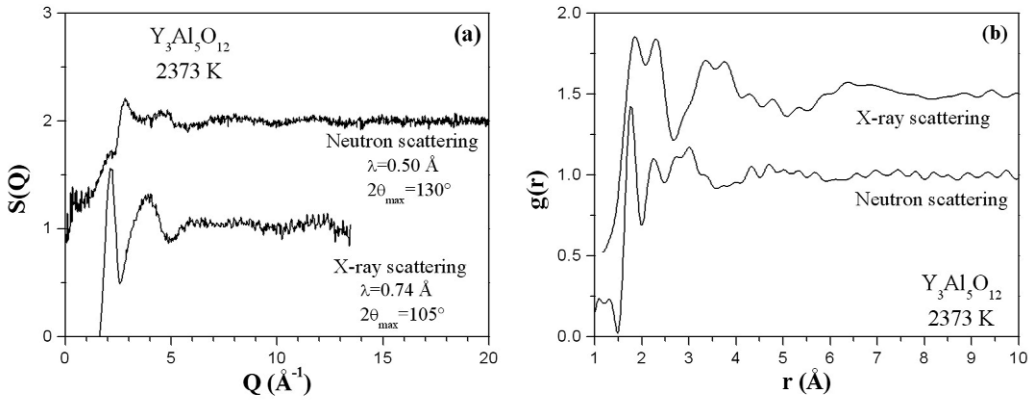

Fig. 4 (a) Structure factor $S(Q)$ for liquid YAG at 2373 K measured using X-ray and neutron scattering. (b) Corresponding X-ray and neutron pair correlation functions $g(r)$. In both cases, curves are shifted up for clarity.

Table 1 X-ray and neutron weighting factors for $Y_3Al_5O_{12}$ (YAG).

	Y-O	Al-O	O-O	Y-Y	Y-Al	Al–Al
Neutrons	0.267	0.198	0.400	0.045	0.066	0.024
X-rays	0.285	0.175	0.129	0.158	0.193	0.060

The X-ray and neutron pair correlation functions $g(r)$ obtained by a Fourier transform of $S(Q)$ are presented in Fig. 4b. The better resolution of the neutron pair correlation function is due to the larger Q

range of $S^N(Q)$ compared to $S^X(Q)$. In both cases, the first two peaks are found at the same position. The first peak at 1.76 Å corresponds to the nearest-neighbor Al-O distance, and the second peak at 2.22 Å is due to Y-O correlations. A Gaussian fit gives Al-O coordination numbers of 4.1 ± 0.5 with neutrons and 4.2 ± 0.5 with X-rays in agreement with a previous X-ray study of liquid YAG [20]. The interpretation of the other peaks is more difficult, since all other correlations are involved.

To go further, it is possible to use more selective methods like the anomalous X-ray scattering technique [21,22]. Some experiments have already been performed, and the data treatment is in progress.

DYNAMICS OF LIQUID REFRACTORY OXIDES

The dynamics of liquids are reasonably well understood in two regimes of length scale L. When L is much longer than interatomic distances, it means at Q values close to zero. In this case, hydrodynamic theory is applied. The other case is when L is of the same order as interatomic distances. It corresponds roughly to Q values above the first peak in $S(Q)$. In this case, we can apply kinetic theory.

The intermediate region remains a challenge for modern statistical physics [23–25]. Kinematic restrictions of neutron scattering make it impossible to reach a certain range of wave vector $\boldsymbol{Q}$, and it is not possible to work at very high temperature with light-scattering techniques like Brillouin spectroscopy because the inelastic signal is masked by the thermal radiation.

The high-resolution inelastic X-ray scattering (IXS) technique goes beyond these limitations and has been largely used to study various liquids including water [26], molecular liquids [27], and metallic melts [28,29]. This method has been recently applied to study levitated liquids [30,31]. For all these studies, the data interpretation is based on generalized hydrodynamics, which is an extension of the classical hydrodynamics with a frequency dependence of the transport coefficients like the viscosity.

Theoretical background

In an IXS experiment, the intensity is given by the convolution of the dynamic structure factor $S(Q,\omega)$ with the resolution function $R(\omega)$. An angle-dependent factor $A(Q)$ is also applied:

$$I(Q,\omega) = A(Q)R(\omega) \otimes S(Q,\omega) \tag{5}$$

At low Q, typical IXS spectra exhibit a triplet including a central Rayleigh peak and two lateral Brillouin peaks. In the generalized hydrodynamic theory, $S(Q,\omega)$ can be written as a sum of three Lorentzians where Γ is the width of the central peak, Γ_S and ω_S are the width and frequency of the Brillouin peaks:

$$S(Q,\omega) = S(Q)e^{\frac{\hbar\omega}{2kT}} \frac{1}{\pi}\left[A_0 \frac{\Gamma}{\omega^2+\Gamma^2} + A_S \frac{\Gamma_S + b(\omega+\omega_S)}{(\omega+\omega_S)^2+\Gamma_S^2} + A_S \frac{\Gamma_S - b(\omega-\omega_S)}{(\omega-\omega_S)^2+\Gamma_S^2} \right] \tag{6}$$

The frequencies of the Brillouin peak, renormalized by the damping term, have a linear Q dependence, and the slope gives directly the sound speed:

$$\Omega_S = \sqrt{\omega_S^2 + \Gamma_S^2} = v_S Q \tag{7}$$

To determine the longitudinal viscosity, we applied a two-time-scale model. In this formalism, thermal fluctuations are neglected and the density fluctuations are described by a slow process following a Debye law (exponential decay) and a fast process quasi-instantaneous. In this case, the longitudinal viscosity is given by:

$$\eta_l = \eta_\infty + \frac{\eta_0}{1 + i\omega\tau} \tag{8}$$

where the first term is related to the width of Brillouin peaks and the second term is associated to the width of the Rayleigh peak.

Experiment

The levitation set-up will be described in detail in a forthcoming paper. It was mounted on the ID16 beamline at ESRF (Grenoble, France) [32]. The incident beam with an energy of 21.747 keV is obtained by the (11,11,11) reflection on a silicon monochromator operating in a back-scattering mode. The scattered photons are collected by five spherically bended Si crystals, making it possible to measure five Q positions simultaneously. Measurements were performed in the 1–15 nm^{-1} Q range.

The energy resolution of the spectrometer was measured using a Plexiglas® sample. This material acts as a purely elastic scatterer with a negligible width in the elastic peak, thus, its spectrum represents the energy resolution function of the instrument.

Figure 5a shows the inelastic X-ray scattering spectra for liquid $MgAl_2O_4$ at three values of the wave vector Q. Measurements were performed above the melting point at a temperature of 2423 K. Figure 5b shows the linear Q dependence of Ω_s. The linear fit gives a sound velocity of 6380 ± 150 m/s.

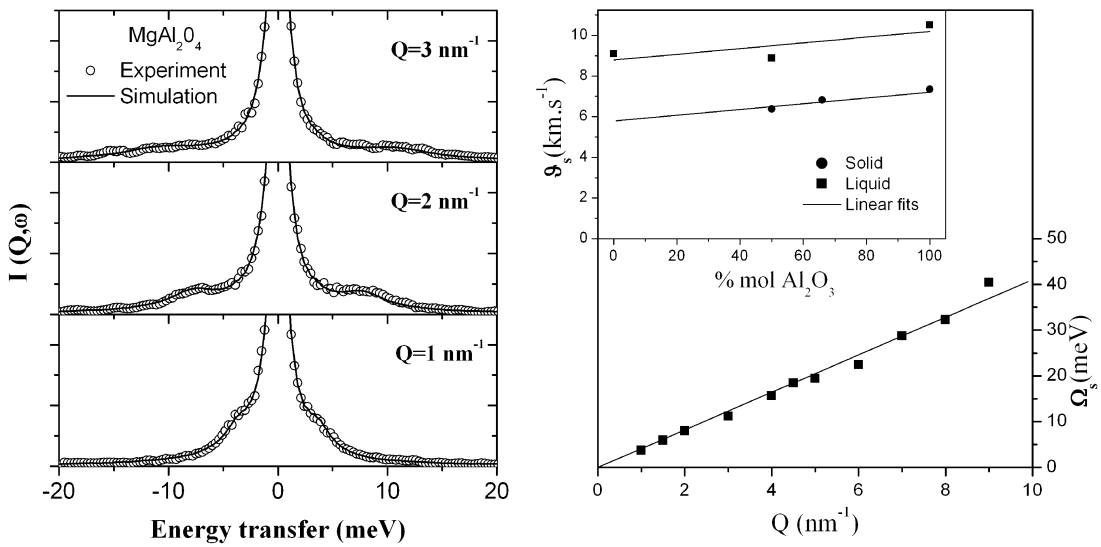

Fig. 5 (a) Selected IXS spectra for liquid $MgAl_2O_4$ (circles) at three Q values. The plain line is the fit using the two-time-scale model. (b) Q dependence of the frequency Ω_s of the Brillouin peaks for liquid $MgAl_2O_4$. The inset shows the composition dependence of the longitudinal sound velocity for solid and liquid $(MgO)_{1-x}(Al_2O_3)_x$ compounds. The solid lines are linear fits.

IXS spectra were fitted using the two-time-scale model, and results are also reported in Fig. 5a using plain lines. From theses fits, we determined a longitudinal viscosity of η_l = 60 mPas.s. The relaxation time of the slow process is found to be around 0.9 ps.

The inset of the figure shows the evolution of the sound velocity above the melting point of $(MgO)_{1-x}(Al_2O_3)_x$ compounds for the composition x = 0.5, 66.6, and 1. The evolution is quasi-linear and has the same behavior as the speed of sound in the solid with a ratio liquid/solid around 0.7.

This two-time-scale model works well in this case, but cannot be used systematically. Very often, it is necessary to introduce a second relaxation time [33].

SUMMARY

The use of containerless techniques enables studies of materials above the melting point and in the supercooled state with a high degree of control. In particular, the atomic structure of liquid materials can be determined by measurements of the X-ray structure factor $S(Q)$ and calculation of the corresponding pair correlation function $g(r)$. Of the different containerless methods, aerodynamic levitation combined with laser heating has proved to be a powerful and versatile technique for studying the structure, dynamics, and macroscopic properties of high-temperature liquids including insulating compounds (glasses, ceramics, and oxides) and metallic materials.

In most cases, the studied material has more than one element and the interpretation of the results is not easy because $S(Q)$ and $g(r)$ are weighted averages of the corresponding partial functions for the different element pairs. It is then particularly useful to have several determinations of $S(Q)$ and $g(r)$ by using X-ray and neutron scattering. It is also possible to use more selective methods like the anomalous X-ray scattering technique [34,35]. The recent developments at IXS beamlines make it possible to study the dynamics of levitated liquids and access information not previously accessible.

ACKNOWLEDGMENTS

The authors wish to thank the APS, ESRF, and ILL staff for their help with the experiments. This work was partially supported by the U.S. Department of Energy, Office of Science, Office of Basic Energy Sciences, under contract no. W-31-109-ENG-38, the CNRS, and the regional council of the Région Centre.

REFERENCES

1. G. Jacobs, I. Egry, K. Maier, D. Platzek, J. Reske, R. Frahm. *Rev. Sci. Instrum.* **67**, 3683 (1996).
2. P. F. Paradis, T. Ishikawa, J. Yu, S. Yoda. *Rev. Sci. Instrum*. **72**, 2811 (2001).
3. E. H. Trinh, C. J. Hsu. *J. Acoust. Soc. Am.* **6**, 1757 (1986).
4. P. H. Haumesser, J. P. Garandet, J. Bancillon, M. Daniel. *Int. J. Thermophys*. **23**, 1277 (2002).
5. L. Hennet, D. Thiaudière, M. Gailhanou, C. Landron, J.-P. Coutures, D. L. Price. *Rev. Sci. Instrum*. **73**, 124 (2002).
6. L. Hennet, I. Pozdnyakova, A. Bytchkov, V. Cristiglio, P. Palleau, H. E. Fischer, G. J. Cuello, M. Johnson, P. Melin, D. Zanghi, S. Brassamin, J.-F. Brun, D. L. Price, M.-L. Saboungi. *Rev. Sci. Instrum*. **77**, 053903 (2006).
7. S. Ansell, S. Krishnan, J. K. R. Weber, J. J. Felten, P. C. Nordine, M. A. Beno, D. Price, M. L. Saboungi. *Phys. Rev. Lett.* **78**, 464 (1997).
8. S. Krishnan, S. Ansell, J. J. Felten, K. J. Volin, D. L. Price. *Phys. Rev. Lett*. **81**, 586 (1998).
9. C. Landron, L. Hennet, T. Jenkins, G. N. Greaves, J. P. Coutures, A. Soper. *Phys. Rev. Lett*. **86**, 4839 (2001).
10. H. E. Fischer, A. C. Barnes, P. S. Salmon. *Rep. Prog. Phys.* **69**, 233 (2006).
11. D. Waasmaier, A. Kirfel. *Acta Crystallogr., Sect. A* **51**, 416 (1995).
12. S. Sasaki. KEK Report 88-14, p. 1 (1989).
13. V. F. Sears. *Neutron News* **3**, 26 (1992).
14. S. Krishnan, D. L. Price. *J. Phys.: Condens. Matter* **12**, R145 (2000).
15. H. E. Fischer, G. J. Cuello, P. Palleau, D. Feltin, A. C. Barnes, Y. S. Badyal, J. M. Simonson. *Appl. Phys. A* **74**, S160 (2002).

16. C. Landron, L. Hennet, J. P. Coutures, T. Jenkins, C. Aletru, N. Greaves, A. K. Soper, G. Derbyshire. *Rev. Sci. Instrum*. **71**, 1745 (2000).
17. T. Schenk, D. Holland-Moritz, V. Simonet, R. Bellissent, D. M. Herlach. *Phys. Rev. Lett.* **89**, 75507 (2002).
18. D. L. Yu, D. Y. Tang. *Opt. Laser Technol.* **35**, 37 (2003).
19. G. Bressi, G. Carugno, E. Conti, C. Del Noce, D. Iannuzzi. *Nucl. Instrum. Meth. Phys. Res., Sect. A* **461**, 361 (2001).
20. J. K. R. Weber, S. Krishnan, S. Ansell, A. D. Hixson, P. C. Nordine. *Phys. Rev. Lett.* **84**, 3622 (2000).
21. L. Hennet, D. Thiaudière, C. Landron, P. Melin, D. L. Price, J. P. Coutures, J.-F. Bérar, M. L. Saboungi. *Appl. Phys. Lett.* **83**, 3305 (2003).
22. L. Hennet, D. Thiaudière, C. Landron, J.-F. Bérar, M.-L. Saboungi, G. Matzen, D. L. Price. *Nucl. Instrum. Meth. Phys. Res., Sect. B* **207**, 447 (2003).
23. P. A. Egelstaff. *An Introduction to the Liquid State*, Clarendon Press, Oxford (1992).
24. U. Balucani, M. Zoppi. *Dynamics of the Liquid State*, Clarendon Press, Oxford (1994).
25. D. L. Price, M.-L. Saboungi, F. J. Bermejo. *Rep. Prog.Phys.* **66**, 407 (2003).
26. G. Monaco, A. Cunsolo, G. Ruocco, F. Sette. *Phys. Rev. E* **60**, 5505 (1999).
27. E. Pontecorvo, R. Di Leonardo, C. Masciovecchio, G. Ruocco, B. Ruzicka, T. Scopigno, F. Sette. *Pure Appl. Chem*. **76**, 79 (2004).
28. T. Scopigno, U. Balucani, G. Ruocco, F. Sette. *Phys. Rev. E* **63**, 011210 (2000).
29. F. Sette, G. Ruocco, A. Cunsolo, C. Masciovecchio, G. Monaco, R. Verbeni. *Phys. Rev. Lett.* **84**, 4136 (2000).
30. H. Sinn, B. Glorieux, L. Hennet, A. Alatas, M. Hu, E. E. Alp, F. J. Bermejo, D. L. Price, M.-L. Saboungi. *Science* **299**, 2047 (2003).
31. A. Alatas, A. H. Said, H. Sinn, E. E. Alp, C. N. Kodituwakku, B. Reinhart, M.-L. Saboungi, D. L. Price. *J. Phys. Chem. Solids* **66**, 2230 (2005).
32. R. Verbeni, F. Sette, M. H. Krisch, U. Bergmann, B. Gorges, C. Halcoussis, K. Martel, C. Masciovecchio, J. F. Ribois, G. Ruocco, H. Sinn. *J. Synch. Rad.* **3**, 62 (1996).
33. T. Scopigno, G. Ruocco, F. Sette. *Rev. Mod. Phys*. **77**, 881 (2005).
34. L. Hennet, D. Thiaudière, C. Landron, P. Melin, D. L. Price, J. P. Coutures, J.-F. Bérar, M. L. Saboungi. *Appl. Phys. Lett.* **83**, 3305 (2003).
35. L. Hennet, D. Thiaudière, C. Landron, J.-F. Bérar, M.-L. Saboungi, G. Matzen, D. L. Price. *Nucl. Instrum. Meth. Phys. Res. B* **207**, 447 (2003).